Supporting Information: Elucidating the carbochromism of $K_3[V(O_2)_4]$ with ab initio modeling

Jacob S. Hirschi, Zhiwei Mao, Anjali Verma, M. A. Subramanian, May Nyman, and Tim J. Zuehlsdorff*

Department of Chemistry, Oregon State University, Corvallis, Oregon 97331, United States

E-mail: tim.zuehlsdorff@oregonstate.edu

Contents

1—Experimental Color Details

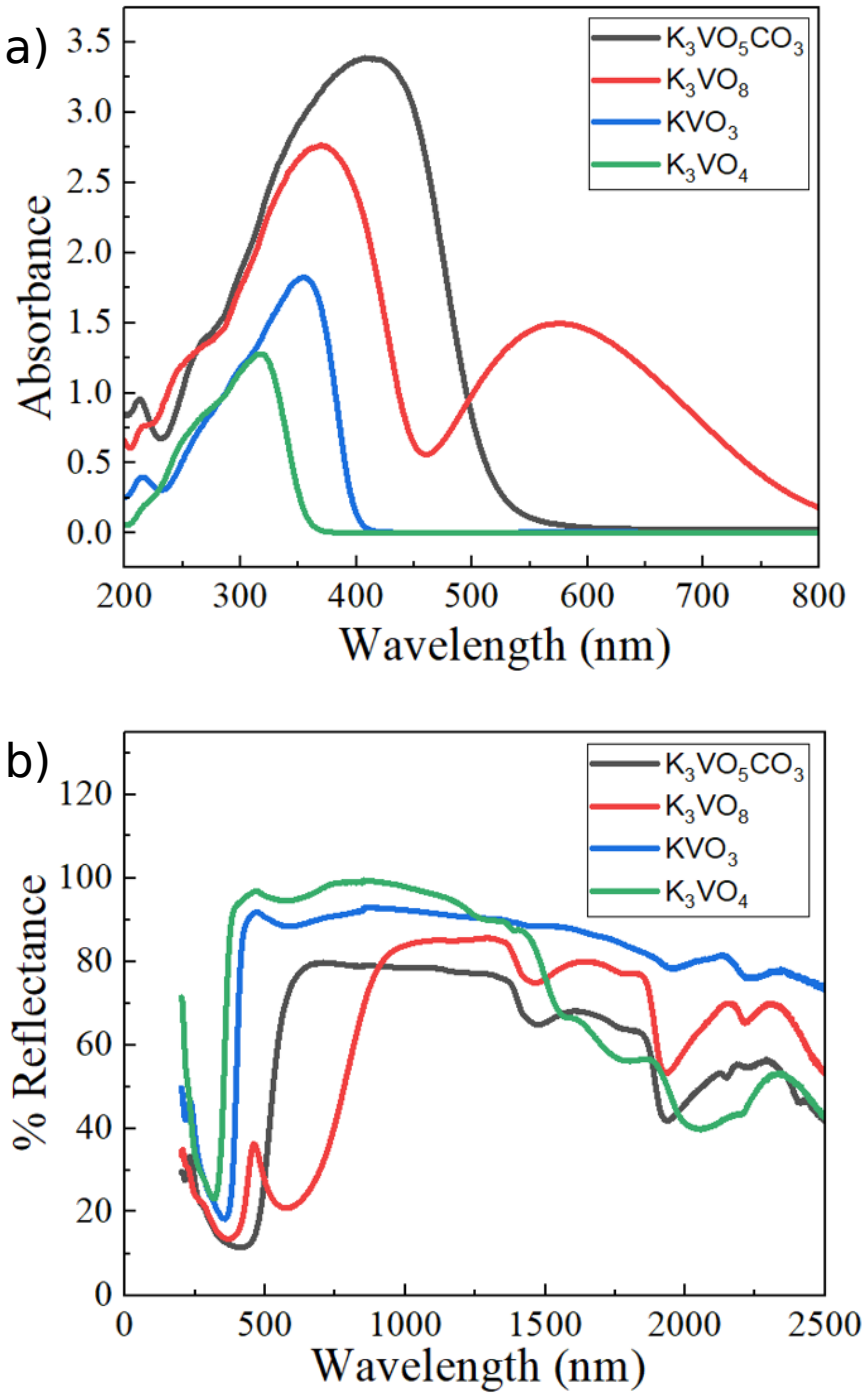

Figure S1: Experimental (a) Kubelka-Munk absorbance and (b) diffuse reflectance spectra. The orthovanadate sample, $K_3[VO_4]$, exhibited similar properties to the metavanadate and was not considered further.

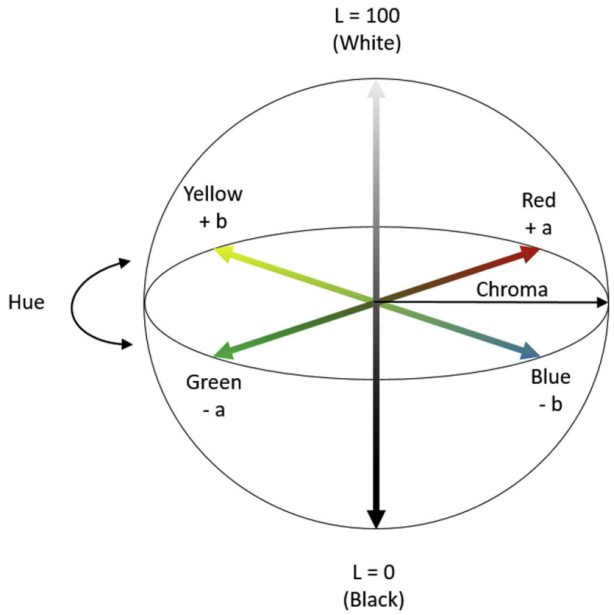

Figure S2: CIE L*a*b* color space. Reproduced with permission from ref. S1.

Table S1: CIE 1976 L*a*b* and sRGB color coordinates from experiment and theory. Computed with a D65 illumninant and CIE 1931 2° Standard Observer functions.

Material	$K_3[V(O_2)_4]$		$K_3[VO(O_2)_2(CO_3)]$		$K[VO_3]$	
	Expt.	Sim.	Expt.	Sim.	Expt.	Sim.
L*	54.86	60.15	81.64	86.69	95.63	99.98
a*	3.06	9.44	3.25	3.09	-0.39	-0.28
b*	-12.42	-22.71	61.25	63.14	-0.71	0.65
C*	12.79	24.59	61.34	63.22	0.81	0.71
h°	283.8	292.6	86.96	87.20	241.2	113.3
$\Delta E^*_{Expt\text{-}Sim}$	13.21		5.39		4.56	
sR	126	141	241	255	241	255
sG	131	141	198	212	243	255
sB	153	185	83	93	244	254

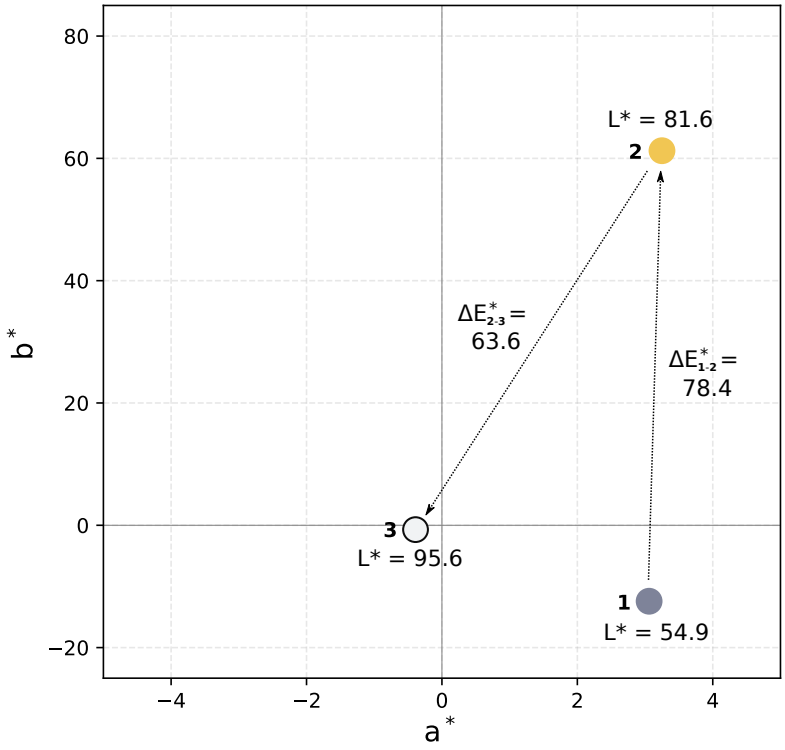

Figure S3: Change in experimental CIE L*a*b* color coordinates from **1** to **2** to **3**.

2—Tauc Plots

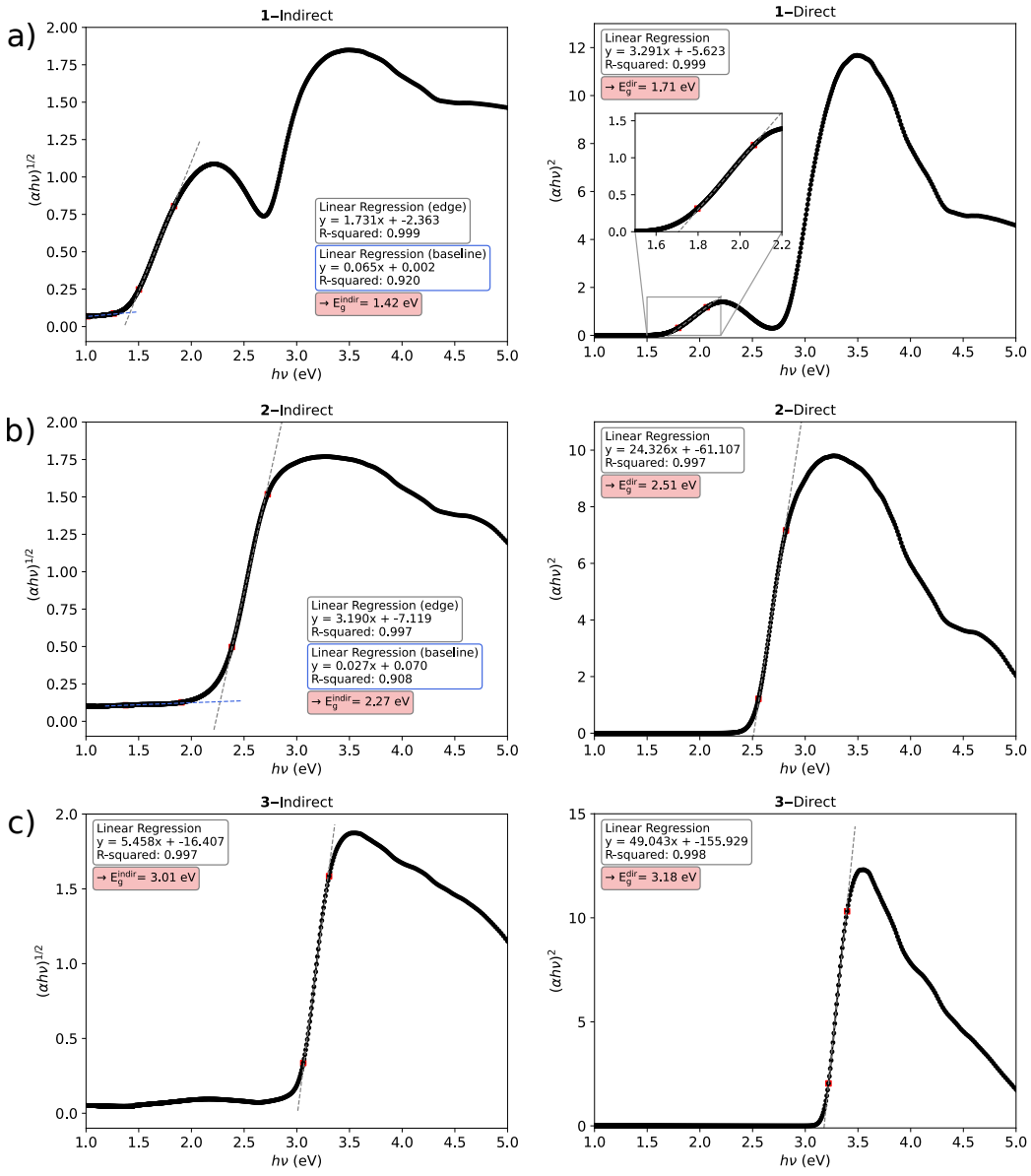

Figure S4: Tauc plots from experimental absorption spectra assuming indirect and direct transitions for (a) **1**, (b) **2**, and (c) **3**.

3—Computational Details

Data Availability

To ensure computational reproducibility, all structures used in this work along with input files have been made available with metadata on a public GitHub repository (`https://github.com/tjz21/DAC_Color`) and on Zenodo (`https://doi.org/10.5281/zenodo.17136901`).

DFT Parameters

Table S2: Exchange-correlation functional and k-grid combinations.

		Structure		
Calculation	XC Functional	$K_3[V(O_2)_4]$	$K_3[VO(O_2)_2(CO_3)]$	$K[VO_3]$
Optimization	rSCAN	3 x 3 x 3	3 x 3 x 3	4 x 2 x 4
Bandstructure	PBE	3 x 3 x 3	3 x 3 x 3	4 x 2 x 4
PDOS/isosurfaces	rSCAN	6 x 6 x 6	6 x 6 x 6	6 x 4 x 6
Absorption	rSCAN	6 x 6 x 6	6 x 6 x 6	6 x 4 x 6

Metal-Oxygen Bonds

Table S3: Selected structural parameters from the computed rSCAN structures.

		r_{avg} (Å), # Occurrences Per Formula	
Bond	$K_3[V(O_2)_4]$	$K_3[VO(O_2)_2(CO_3)]$	$K[VO_3]$
$O-O_{peroxo}$	1.449, 4	1.443, 2	
$V-O_{peroxo}$	1.903, 8	1.888, 4	
$V-O_{carbonato}$		2.033, 2	
$V-O_{oxo}$		1.616, 1	1.720, 4
$V-O_{all,\ avg}$	1.903	1.891	1.720

Color Procedure

The procedure for calculating the color of the powder materials from simulated absorption spectra was modified from published reports on color prediction with molecular systems[S2–S5] and is outlined below.

1. Normalize the maximum absorption intensity to unity in the calculated range, 0 to 30 eV.

2. Transform absorbance into reflectance according to the Kubelka-Munk relationship:[S6]

$$\mathrm{R}_\infty = (\alpha+1) - \sqrt{(\alpha+1)^2 - 1}$$

3. Integrate the reflectance curve against the $\bar{x}, \bar{y}, \bar{z}$ color matching functions and an illuminant factor to account for the spectral distribution of the incident light, yielding XYZ tristimulus values. The CIE 1931 2° Standard Observer functions[S7] and a D65 illuminant were used here.

$$\mathrm{X} = \frac{1}{N}\int_{380\ \mathrm{nm}}^{780\ \mathrm{nm}} (\mathrm{R}_{\mathrm{material}}) \times (\mathrm{Illuminant}) \times (\bar{x})\ \mathrm{d}\lambda$$

$$\mathrm{Y} = \frac{1}{N}\int_{380\ \mathrm{nm}}^{780\ \mathrm{nm}} (\mathrm{R}_{\mathrm{material}}) \times (\mathrm{Illuminant}) \times (\bar{y})\ \mathrm{d}\lambda$$

$$\mathrm{Z} = \frac{1}{N}\int_{380\ \mathrm{nm}}^{780\ \mathrm{nm}} (\mathrm{R}_{\mathrm{material}}) \times (\mathrm{Illuminant}) \times (\bar{z})\ \mathrm{d}\lambda$$

N is an illuminant-dependent constant that normalizes Y to 100, $N = \int_{380\ \mathrm{nm}}^{780\ \mathrm{nm}} (\mathrm{Illum.}) \times \bar{y}\, d\lambda$.

4. Convert CIE 1931 X,Y,Z values into sRGB using the linear transformation matrix[S5]

$$\begin{bmatrix} sR \\ sG \\ sB \end{bmatrix} = \begin{bmatrix} 3.2404542 & -1.5371385 & -0.4985314 \\ -0.9692660 & 1.8760108 & 0.0415560 \\ 0.0556434 & -0.2040259 & 1.0572252 \end{bmatrix} \begin{bmatrix} X \\ Y \\ Z \end{bmatrix}$$

5. Convert CIE 1931 XYZ into CIE 1976 L*a*b* with the following non-linear operations:[S8]

$$L^* = 116 f(Y/Y_n) - 16$$

$$a^* = 500[f(X/X_n) - f(Y/Y_n)]$$

$$b^* = 200[f(Y/Y_n) - f(Z/Z_n)]$$

where for values of $(X/X_n),(Y/Y_n),(Z/Z_n) > (24/116)^3$

$$f(X/X_n) = (X/X_n)^{\frac{1}{3}}$$

$$f(Y/Y_n) = (Y/Y_n)^{\frac{1}{3}}$$

$$f(Z/Z_n) = (Z/Z_n)^{\frac{1}{3}}$$

Alternatively if $(X/X_n),(Y/Y_n),(Z/Z_n) \leq (24/116)^3$, then

$$f(X/X_n) = (841/108)(X/X_n) + 16/116$$

$$f(Y/Y_n) = (841/108)(Y/Y_n) + 16/116$$

$$f(Z/Z_n) = (841/108)(Z/Z_n) + 16/116$$

$X_n, Y_n,$ and Z_n are the X,Y,Z values of the illuminant.

6. Compute the distance between the DFT-derived and experimentally measured L*a*b* coordinates, $\Delta E^*_{\text{Expt–Sim}}$, with the Euclidean distance formula:

$$\Delta E^* = \sqrt{(\Delta L^*)^2 + (\Delta a^*)^2 + (\Delta b^*)^2}$$

Scale the simulated absorption curve and repeat steps 2-4 until $\Delta E^*_{\text{Expt–Sim}}$ is minimized (see Figure S5).

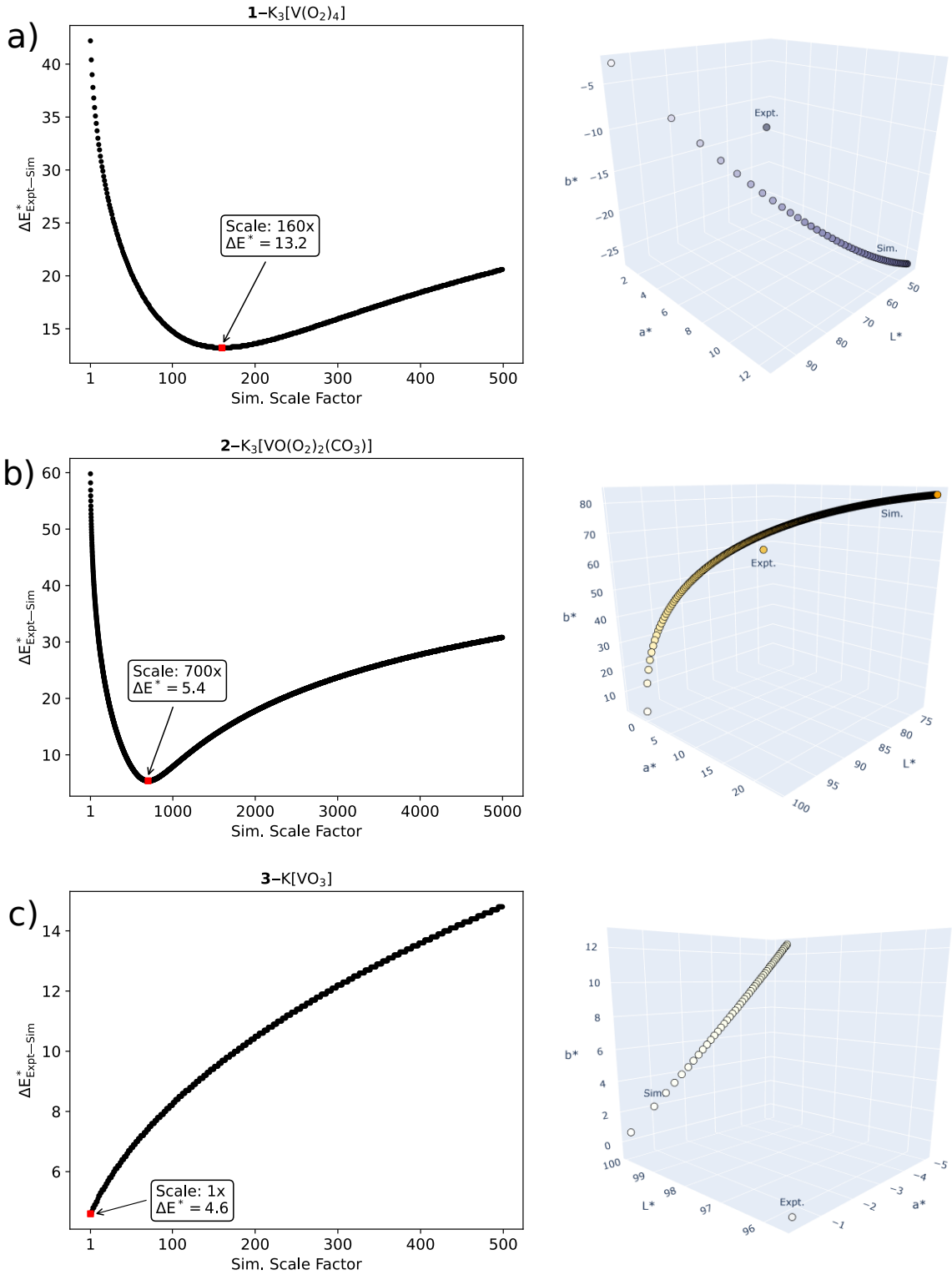

Figure S5: Experimental-simulated color distances as a function of simulated absorbance scaling factors for (a) **1**, (b) **2**, and (c) **3** alongside 3D renderings in CIE L*a*b* coordinates.

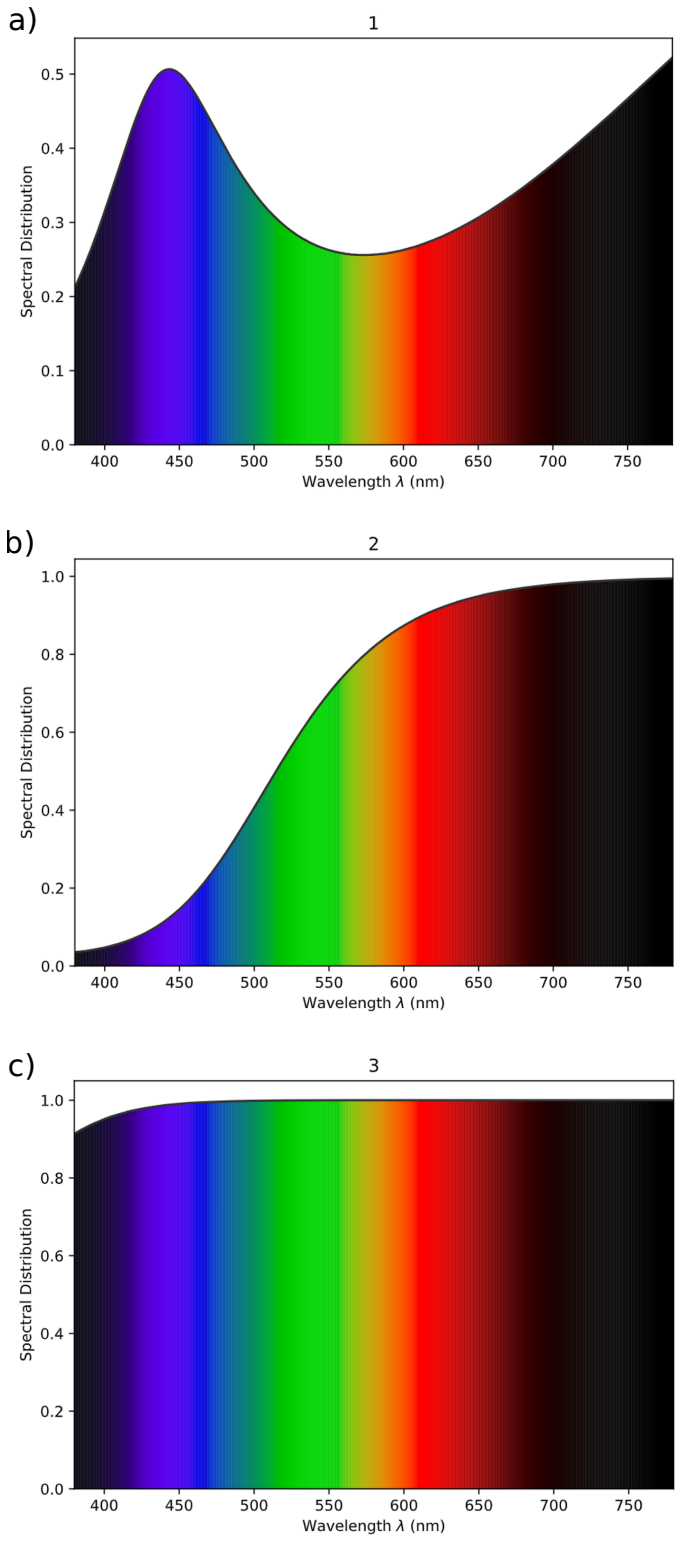

Figure S6: Spectral reflectance curves for (a) $K_3[V(O_2)_4]$ (b) $K_3[VO(O_2)_2(CO_3)]$ and (c) $K[VO_3]$ from scaled computational absorbance spectra (Figure S5)

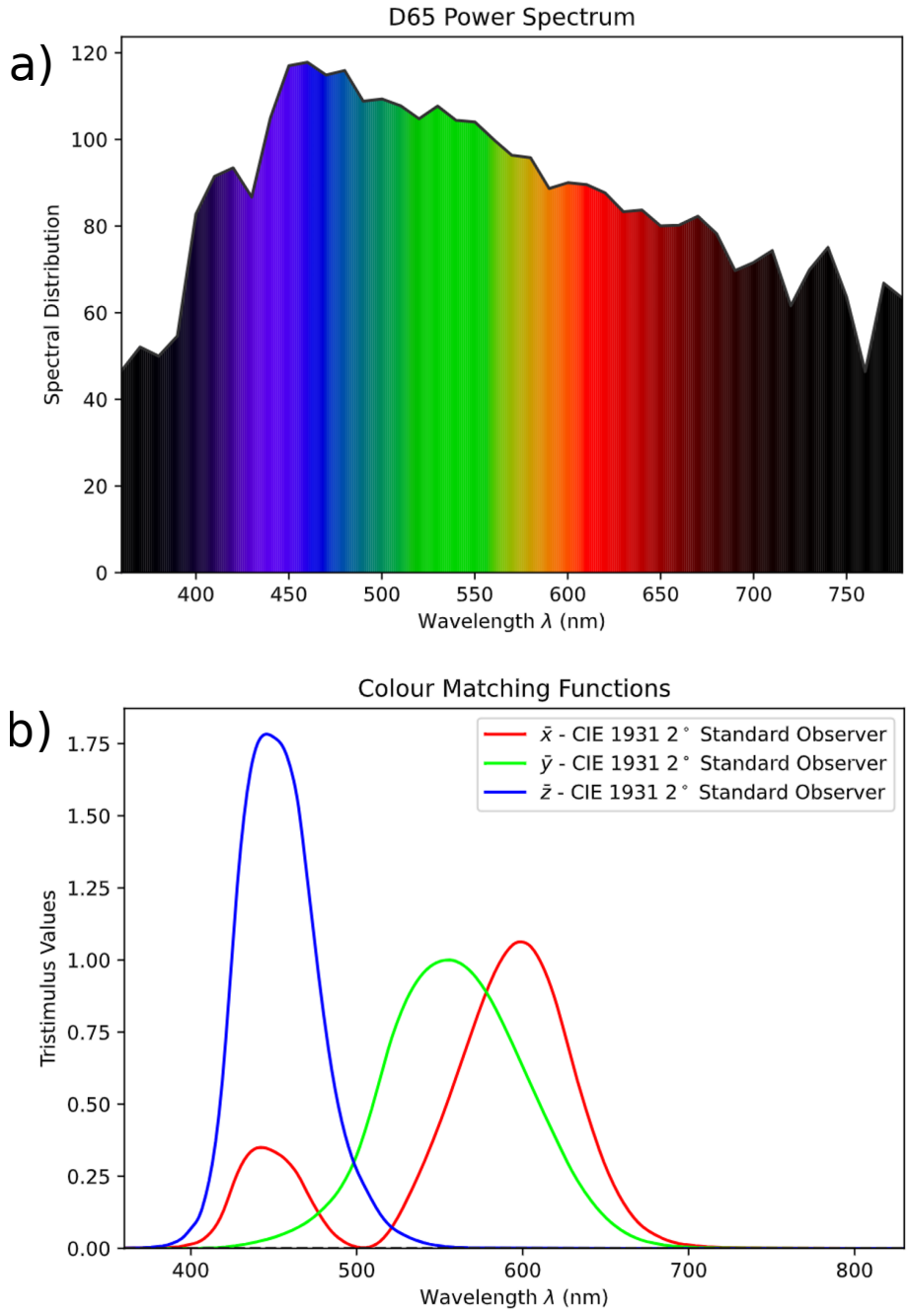

Figure S7: (a) Spectral powder distribution of the standard D65 illuminant, which emulates average noon daylight, and (b) CIE 1931 2° color matching functions used for the color prediction in this work. Both figures were made with the Colour python package.[S9]

4—Full Bandstructure

Full k-point paths through the Brillouin zone for the tetragonal ($I42m$) $K_3[V(O_2)_4]$, mononclinic (Cm) $K_3[VO(O_2)_2(CO_3)]$, and orthorhombic ($Pbcm$) $K[VO_3]$ from the Bradley and Cracknell reference text.[S10]

- $K_3[V(O_2)_4]$: $\Gamma^*\left(0\,0\,0\right) \rightarrow X\left(0\,0\,\frac{1}{2}\right) \rightarrow P\left(\frac{1}{4}\,\frac{1}{4}\,\frac{1}{4}\right) \rightarrow N\left(0\,\frac{1}{2}\,0\right) \rightarrow \Gamma^*\left(0\,0\,0\right) \rightarrow Z\left(\frac{1}{2}\,\frac{1}{2}\,\frac{1}{2}\right)$
- $K_3[VO(O_2)_2(CO_3)]$: $\Gamma\left(0\,0\,0\right) \rightarrow Y\left(\frac{1}{2}\,\frac{1}{2}\,0\right) \rightarrow V\left(\frac{1}{2}\,0\,0\right) \rightarrow \Gamma\left(0\,0\,0\right) \rightarrow A^*\left(0\,0\,\frac{1}{2}\right) \rightarrow M\left(\frac{1}{2}\,\frac{1}{2}\,\frac{1}{2}\right) \rightarrow L\left(\frac{1}{2}\,0\,\frac{1}{2}\right) \rightarrow V\left(\frac{1}{2}\,0\,0\right)$
- $K[VO_3]$: $\Gamma\left(0\,0\,0\right) \rightarrow Z\left(0\,0\,\frac{1}{2}\right) \rightarrow T\left(-\frac{1}{2}\,0\,\frac{1}{2}\right) \rightarrow Y^*\left(-\frac{1}{2}\,0\,0\right) \rightarrow S\left(-\frac{1}{2}\,\frac{1}{2}\,0\right) \rightarrow R\left(-\frac{1}{2}\,\frac{1}{2}\,\frac{1}{2}\right) \rightarrow U\left(0\,\frac{1}{2}\,\frac{1}{2}\right) \rightarrow X\left(0\,\frac{1}{2}\,0\right) \rightarrow \Gamma\left(0\,0\,0\right) \rightarrow Y^*\left(-\frac{1}{2}\,0\,0\right)$

The lowest energy direct transitions occur at k-points denoted with *. Bandstructure diagrams made with sumo[S11] with the VBM shifted to zero. Specific commands used to generate these diagrams are provided on GitHub (`https://github.com/tjz21/DAC_Color/blob/main/computational/plotting_commands.md`).

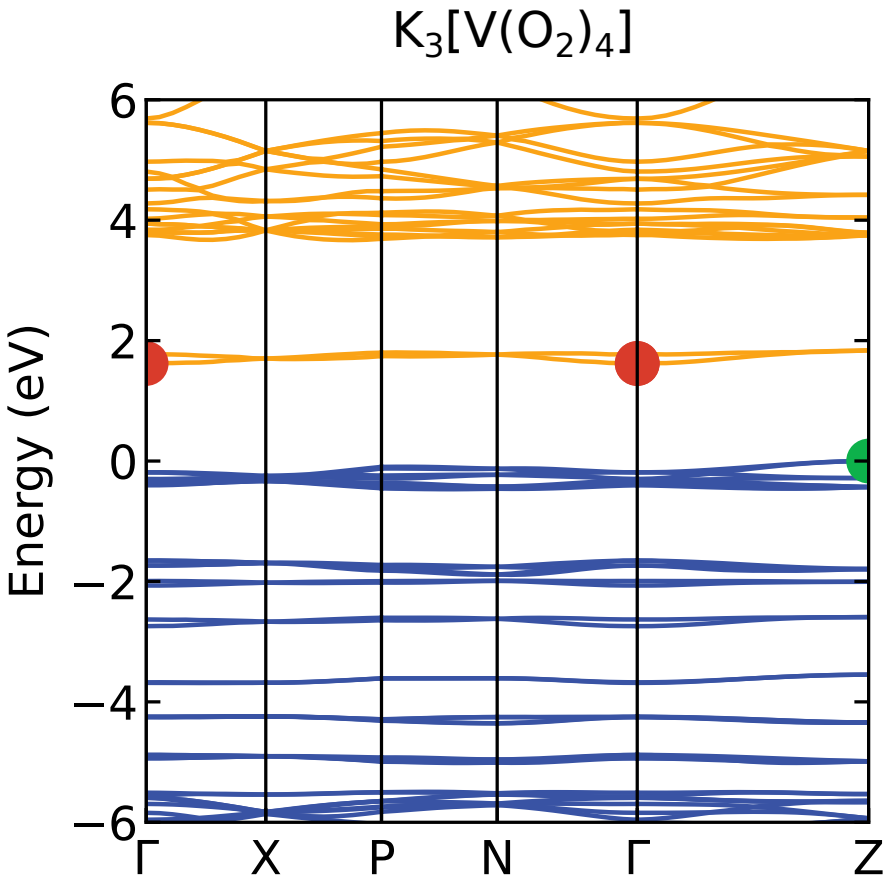

Figure S8: Bandstructure of **1** with occupied and unoccupied bands shown in blue and orange, respectively. Band extrema are depicted as colored dots. Bands were computed with PBE and scissor operated by +0.32 eV to match the indirect rSCAN gap of 1.62 eV ($Z \rightarrow \Gamma$).

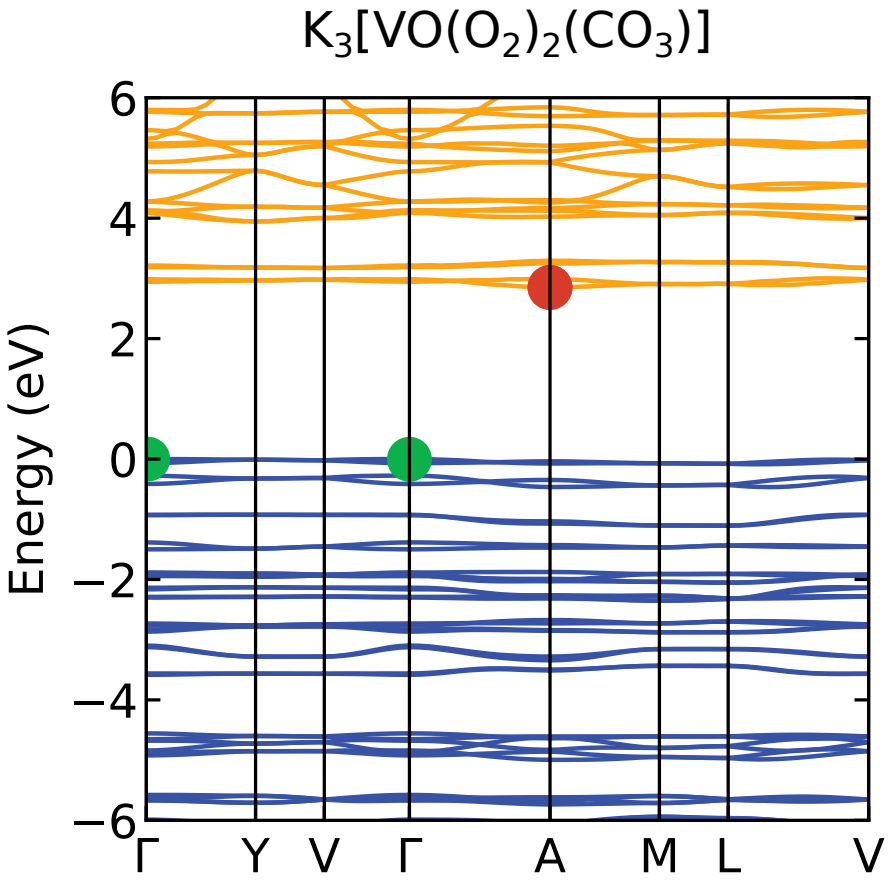

Figure S9: Bandstructure of **2** with occupied and unoccupied bands shown in blue and orange, respectively. Band extrema are depicted as colored dots. Bands were computed with PBE and scissor operated by +0.30 eV to match the indirect rSCAN gap of 2.85 eV ($\Gamma \rightarrow$ A).

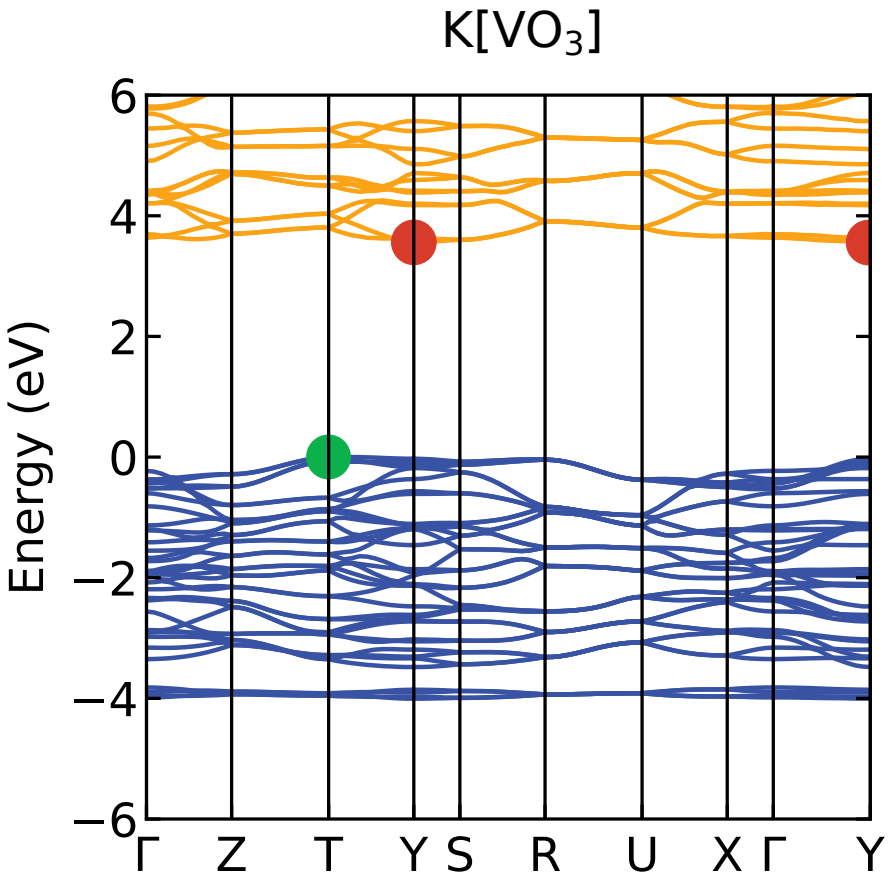

Figure S10: Bandstructure of **3** with occupied and unoccupied bands shown in blue and orange, respectively. Band extrema are depicted as colored dots. Bands were computed with PBE and scissor operated by +0.33 eV to match the indirect rSCAN gap of 3.57 eV (T $\rightarrow$ Y).

5—Extended PDOS

Extended PDOS diagrams from -6 eV to 6 eV were made with sumo[S11] and the VBM were shifted to zero. A gaussian broadening of 0.1 eV was applied. Specific commands used to generate these diagrams are provided on GitHub (`https://github.com/tjz21/DAC_Color/blob/main/computational/plotting_commands.md`).

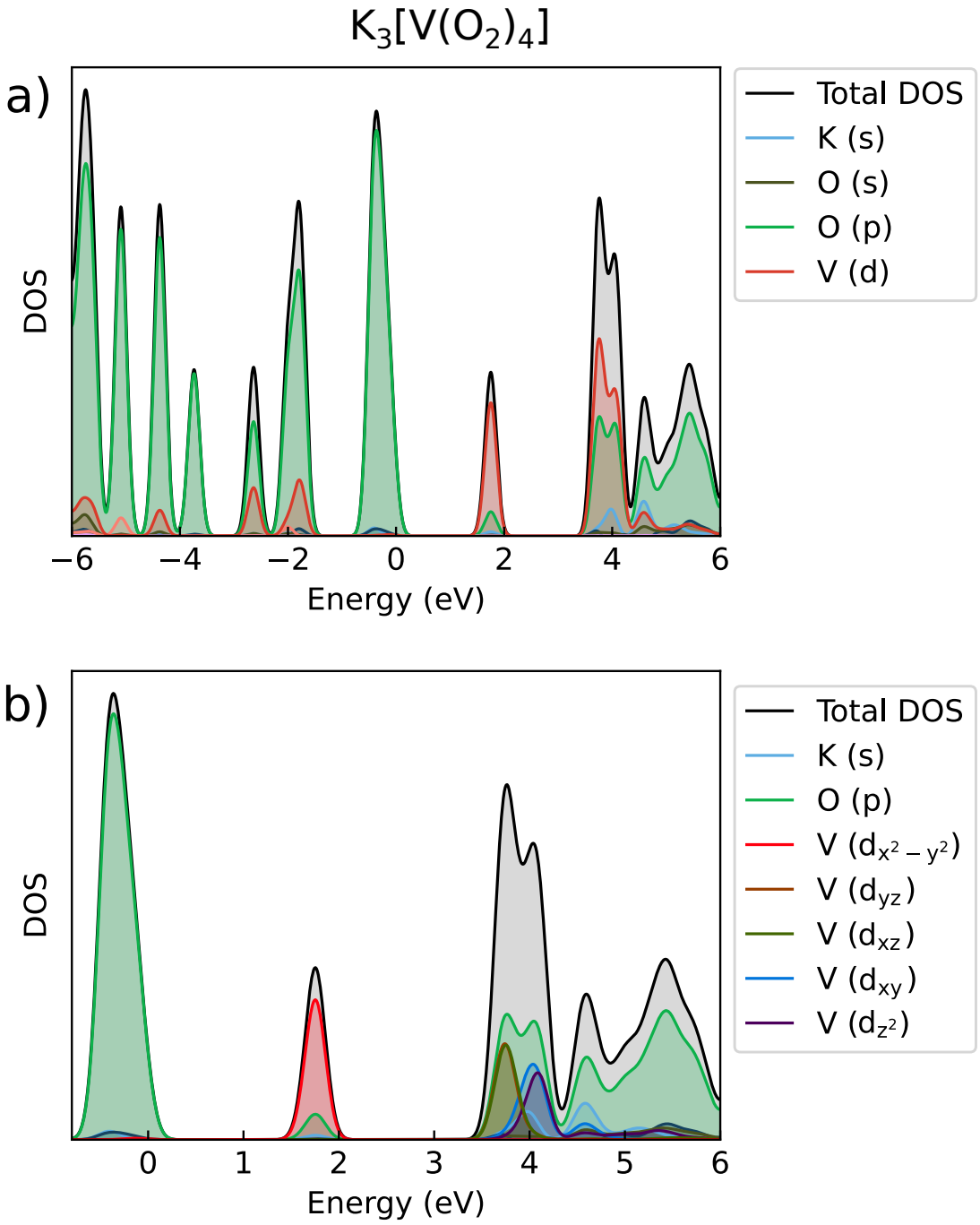

Figure S11: (a) PDOS of $K_3[V(O_2)_4]$ showing atomic contributions, and (b) PDOS with angular momentum projections for vanadium-3d states. Computed with rSCAN.

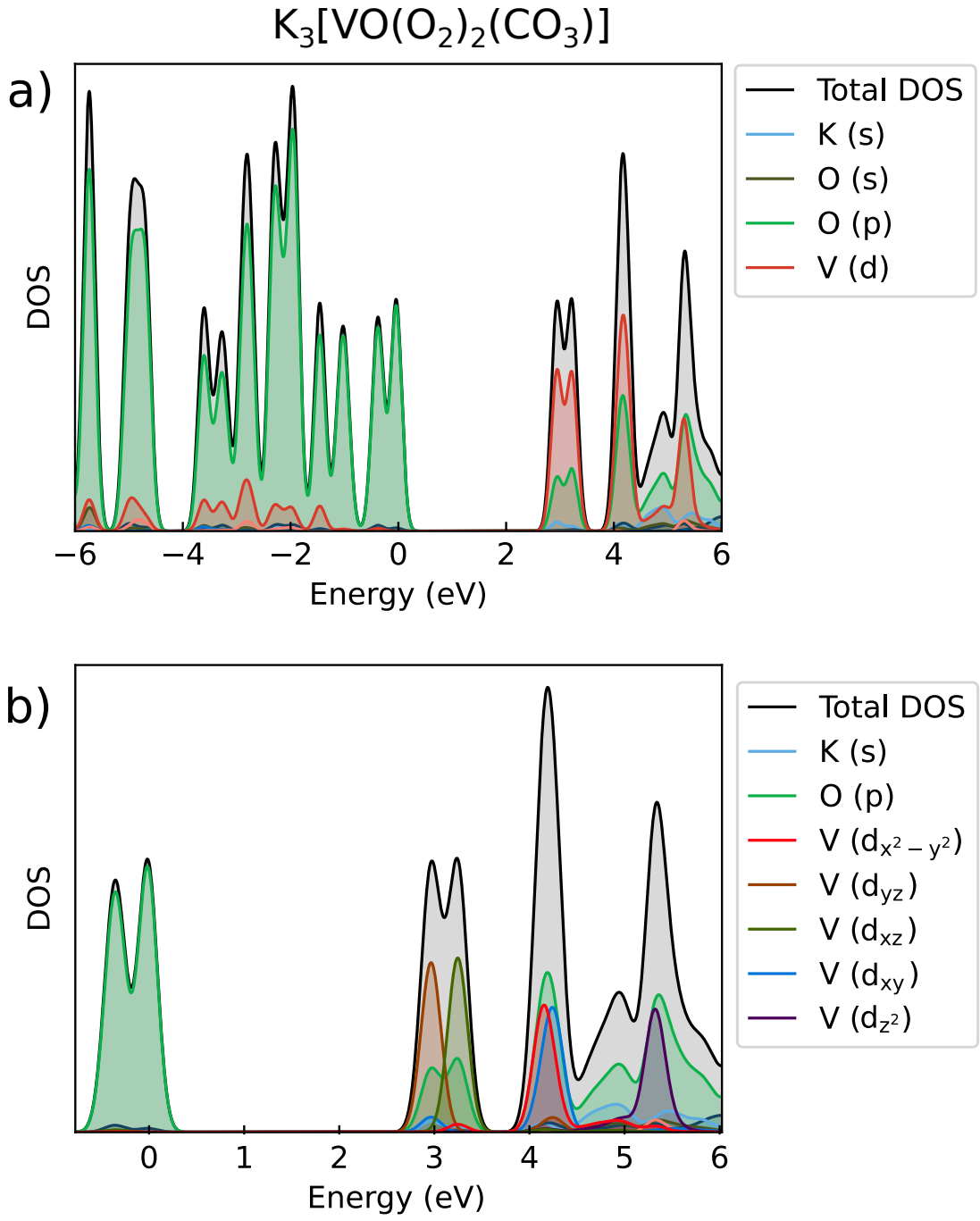

Figure S12: (a) PDOS of $K_3[VO(O_2)_2(CO_3)]$ showing atomic contributions, and (b) PDOS with angular momentum projections for vanadium-3d states. Computed with rSCAN.

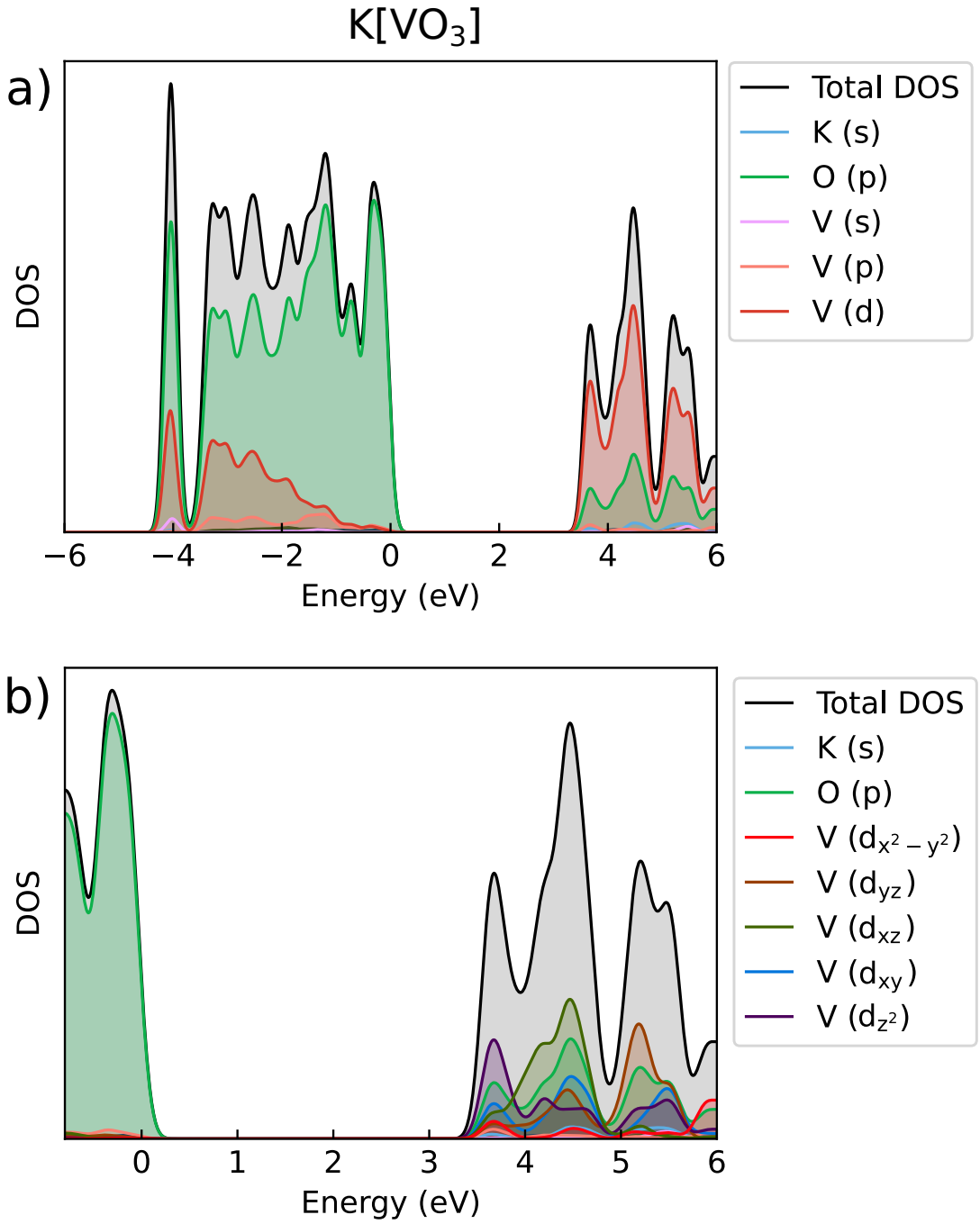

Figure S13: (a) PDOS of $K[VO_3]$ showing atomic contributions, and (b) PDOS with angular momentum projections for vanadium-3d states. Computed with rSCAN.

6—3d Orbital Splitting

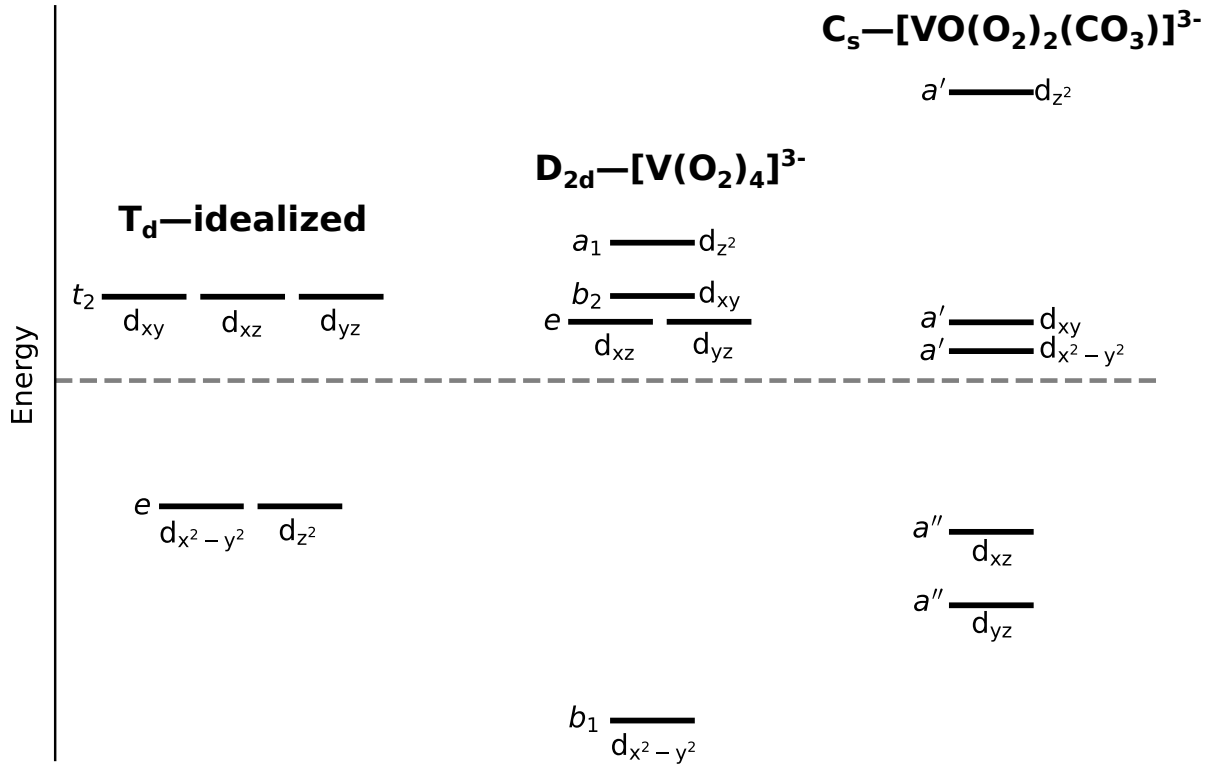

Figure S14: 3d orbital splitting diagram based on the DFT calculations for $K_3[V(O_2)_4]$ and $K_3[VO(O_2)_2(CO_3)]$. The barycenter of the splitting is indicated by a dashed line.

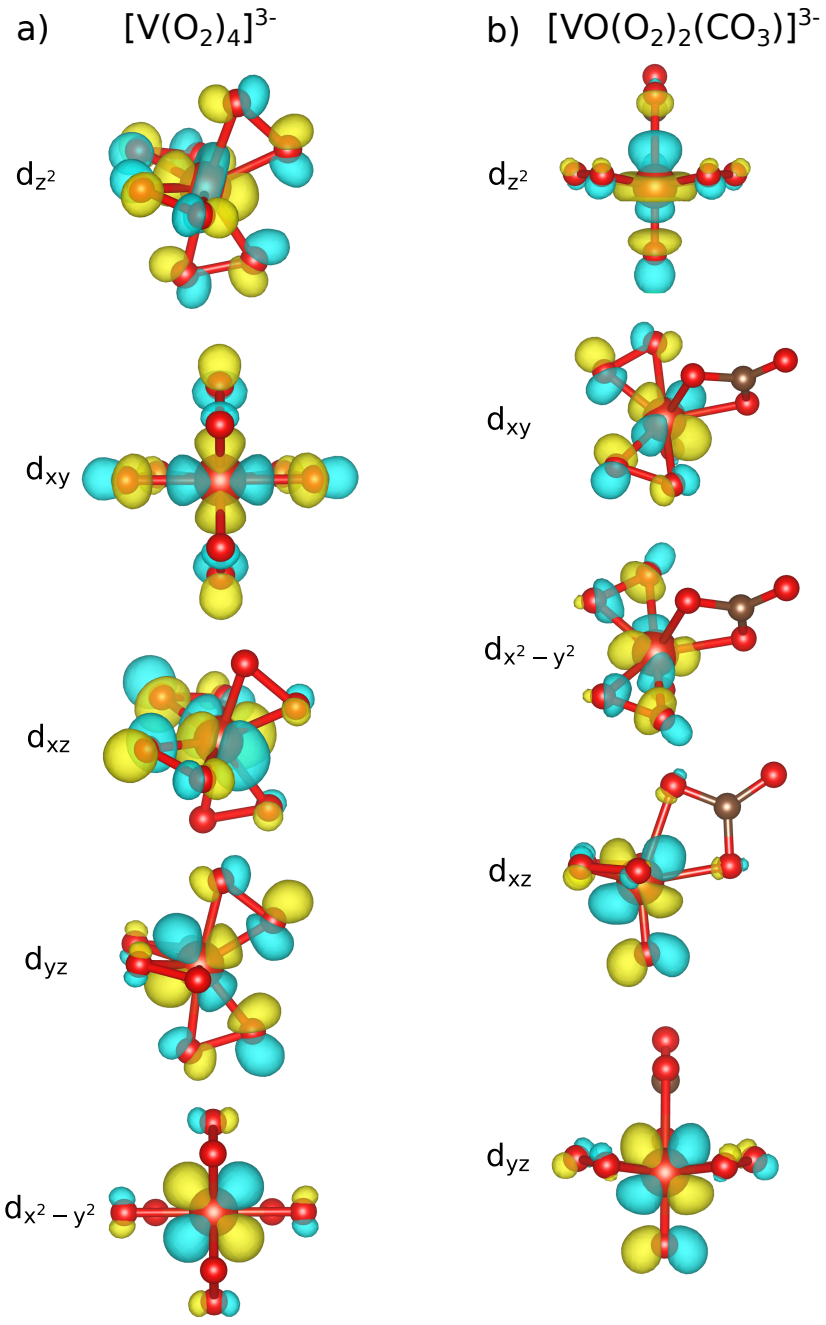

Figure S15: Isosurface renderings of the unoccupied vanadium 3d orbitals in $K_3[V(O_2)_4]$ and $K_3[VO(O_2)_2(CO_3)]$ from rSCAN calculations. Potassium counterions have been omitted for clarity.

7—Functional Benchmarking

Table S4: Direct band gaps from experiment and simulation.

		Direct–E_g (eV)		
Material	Expt.	PBE (% Error)	rSCAN (% Error)	HSE06 (% Error)
1–$K_3[V(O_2)_4]$	1.71	1.44 (-15.6%)	1.82 (+6.4%)	3.55 (+107.4%)
2–$K_3[VO(O_2)_2(CO_3)]$	2.51	2.53 (+0.9%)	2.89 (+15.1%)	4.60 (+83.3%)
3–$K[VO_3]$	3.18	3.22 (+1.2%)	3.59 (+12.9%)	5.00 (+57.5%)

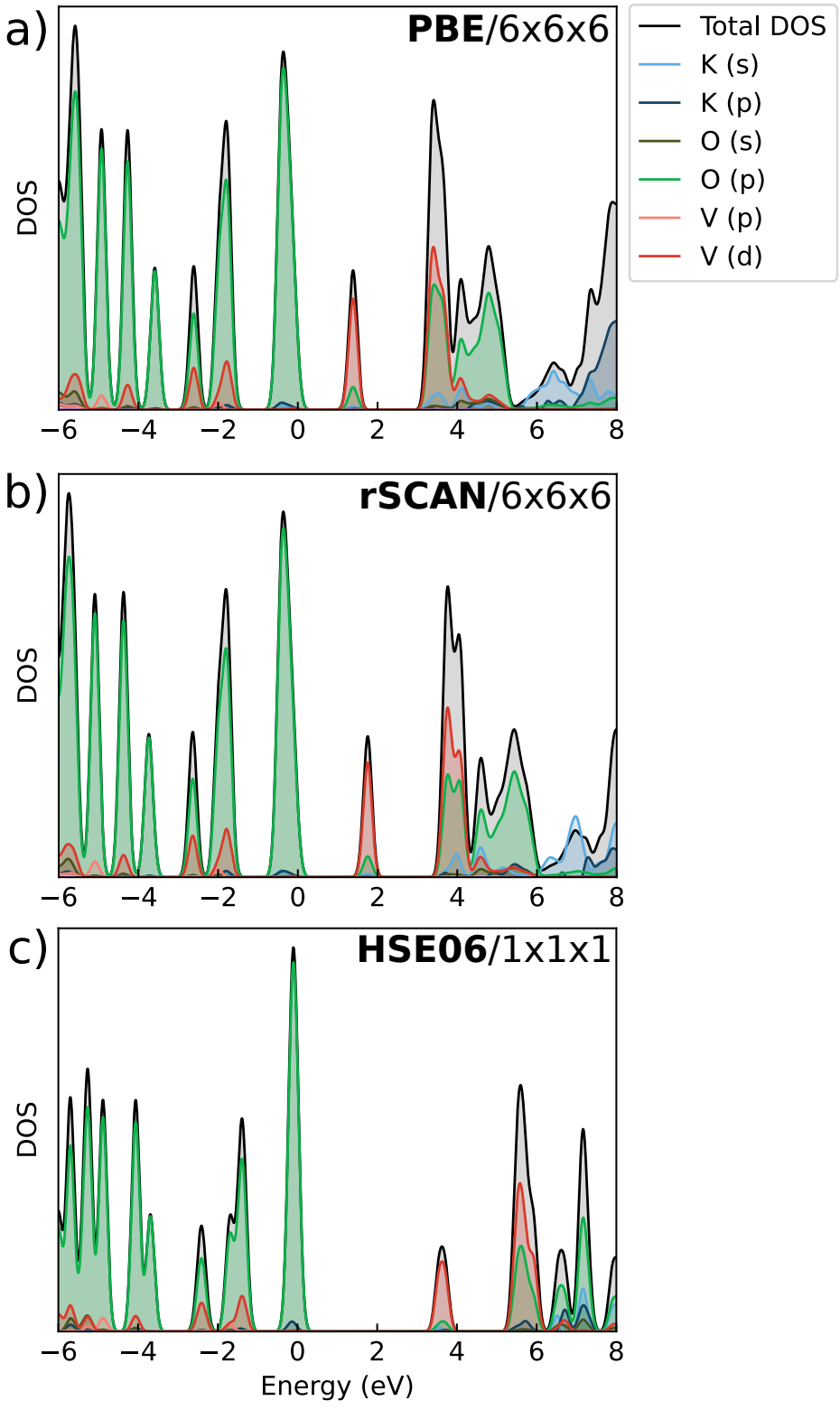

Figure S16: PDOS of $K_3[V(O_2)_4]$ with three functional/k-grid combinations. All computed from the rSCAN/3x3x3 optimized structure.

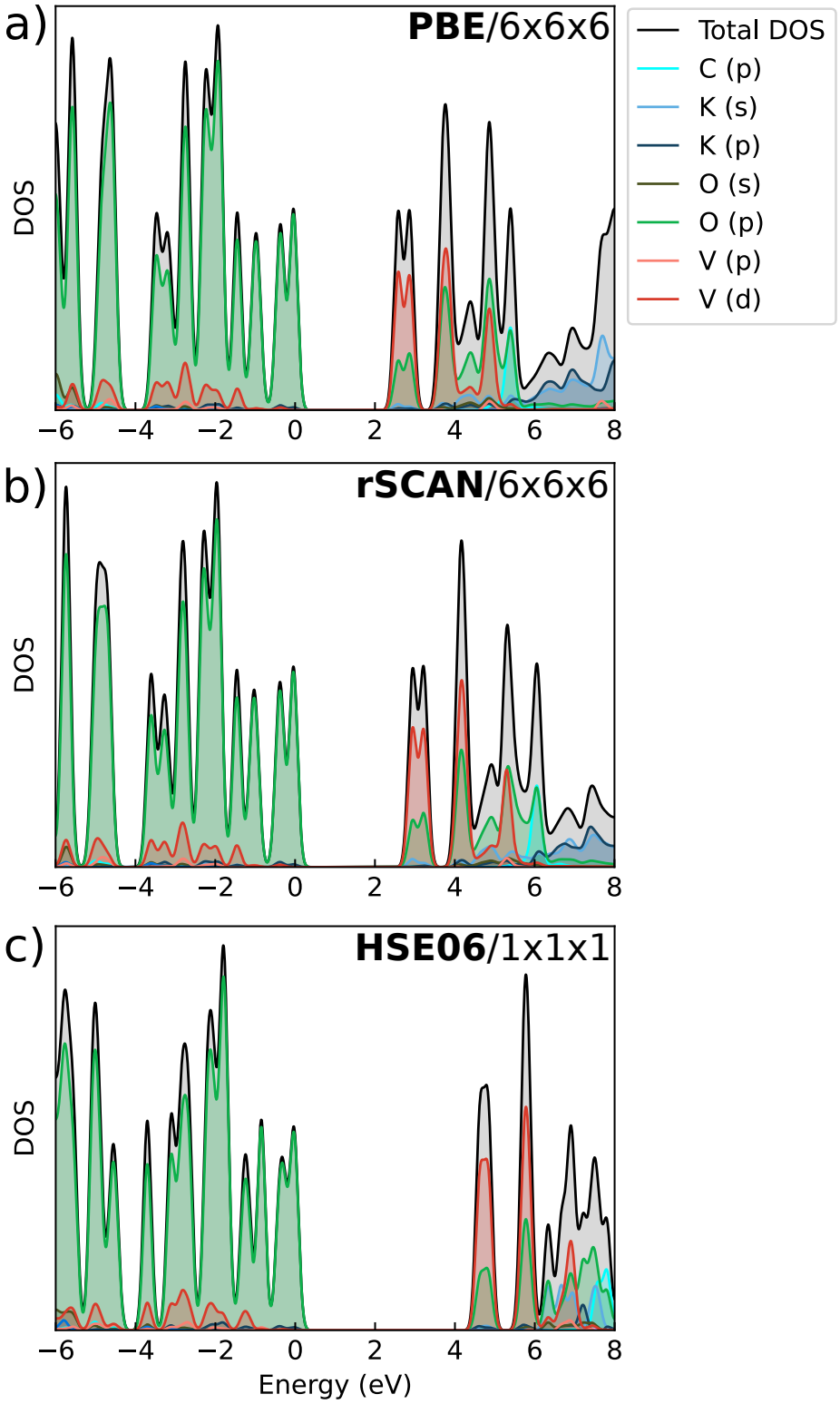

Figure S17: PDOS of $K_3[VO(O_2)_2(CO_3)]$ with three functional/k-grid combinations. All computed from the rSCAN/3x3x3 optimized structure.

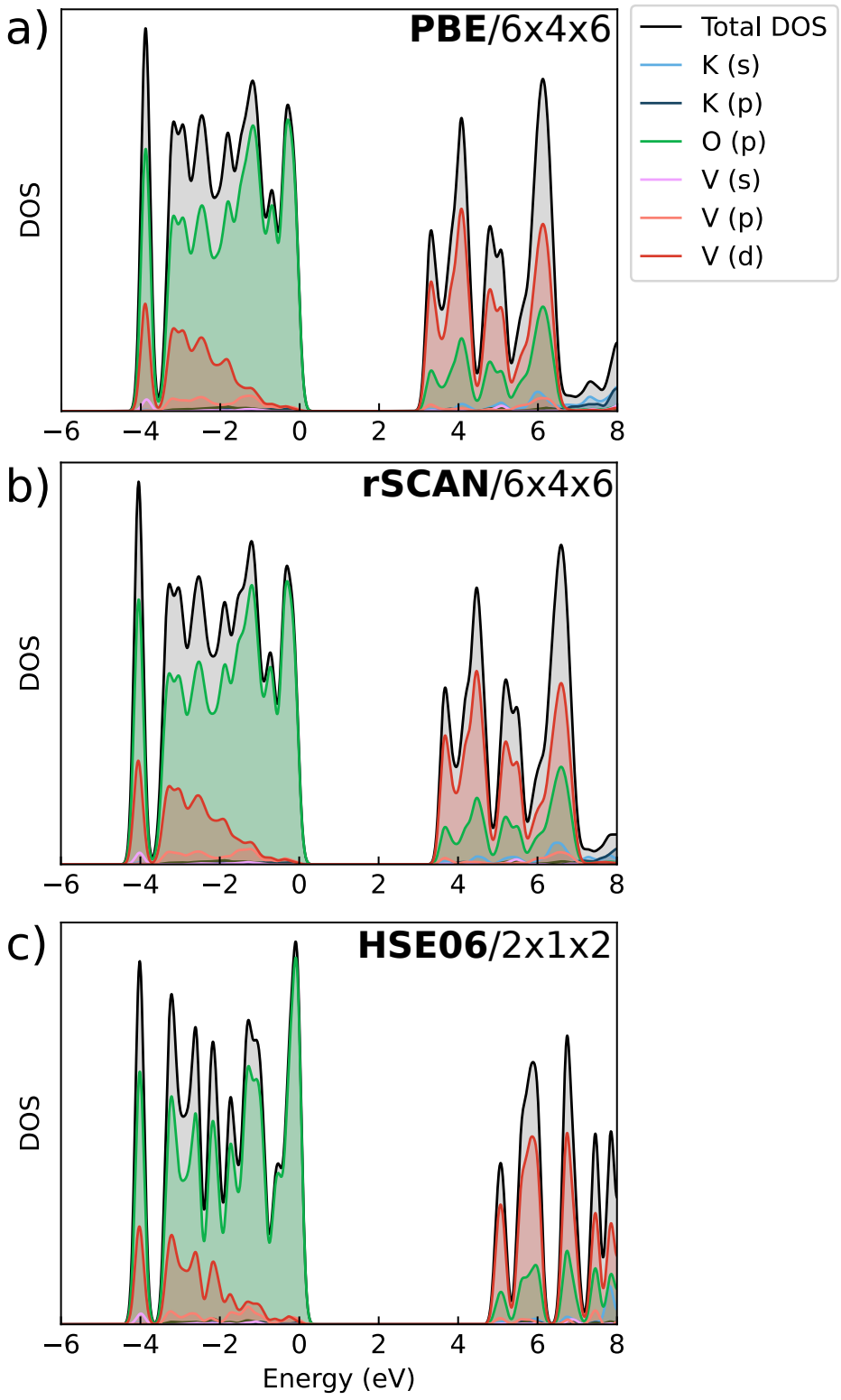

Figure S18: PDOS of K[VO_3] with three functional/k-grid combinations. All computed from the rSCAN/4x2x4 optimized structure.

References

(S1) Ly, B. C. K.; Dyer, E. B.; Feig, J. L.; Chien, A. L.; Del Bino, S. Research Techniques Made Simple: Cutaneous Colorimetry: A Reliable Technique for Objective Skin Color Measurement. *J. Investig. Dermatol.* **2020**, *140*, 3–12, DOI: doi:10.1016/j.jid.2019.11.003.

(S2) Zuehlsdorff, T. J.; Haynes, P. D.; Payne, M. C.; Hine, N. D. M. Predicting solvatochromic shifts and colours of a solvated organic dye: The example of nile red. *J. Chem. Phys.* **2017**, *146*, 124504, DOI: doi:10.1063/1.4979196.

(S3) Ge, X.; Timrov, I.; Binnie, S.; Biancardi, A.; Calzolari, A.; Baroni, S. Accurate and Inexpensive Prediction of the Color Optical Properties of Anthocyanins in Solution. *J. Phys. Chem. A* **2015**, *119*, 3816–3822, DOI: doi:10.1021/acs.jpca.5b01272.

(S4) Malcıoğlu, O. B.; Calzolari, A.; Gebauer, R.; Varsano, D.; Baroni, S. Dielectric and Thermal Effects on the Optical Properties of Natural Dyes: A Case Study on Solvated Cyanin. *J. Am. Chem. Soc.* **2011**, *133*, 15425–15433, DOI: doi:10.1021/ja201733v.

(S5) Williams, D. L.; Flaherty, T. J.; Jupe, C. L.; Coleman, S. A.; Marquez, K. A.; Stanton, J. J. Beyond λmax: Transforming Visible Spectra into 24-Bit Color Values. *J. Chem. Educ.* **2007**, *84*, 1873, DOI: doi:10.1021/ed084p1873.

(S6) Kubelka, P.; Munk, F. An article on optics of paint layers. *Z. Tech. Phys* **1931**, *12*, 259–274.

(S7) Smith, T.; Guild, J. The C.I.E. colorimetric standards and their use. *Trans. Opt. Soc* **1931**, *33*, 73–134, DOI: doi:10.1088/1475-4878/33/3/301.

(S8) Schanda, J. *Colorimetry: Understanding the CIE System*; John Wiley & Sons: Hoboken, NJ, 2007; DOI: doi:10.1002/9780470175637.

(S9) Mansencal, T.; Mauderer, M.; Parsons, M.; Shaw, N.; Wheatley, K.; Cooper, S.; Vandenberg, J. D.; Canavan, L.; Crowson, K.; Lev, O. et al. Colour 0.4.6. 2024; `https://doi.org/10.5281/zenodo.13917514`.

(S10) Bradley, C.; Cracknell, A. *The Mathematical Theory of Symmetry in Solids: Representation Theory for Point Groups and Space Groups*; EBSCO ebook academic collection; OUP Oxford, 2010.

(S11) M Ganose, A.; J Jackson, A.; O Scanlon, D. sumo: Command-line tools for plotting and analysis of periodic ab initio calculations. *J. Open Source Softw.* **2018**, *3*, 717, DOI: doi:10.21105/joss.00717.